Theoretical analysis of ocean color radiances anomalies and implications for phytoplankton groups detection in case 1 waters

S. Alvain,[1,*] H. Loisel,[1] and D. Dessailly[1]

[1]*Université Lille Nord de France, ULCO, LOG, CNRS—UMR8187, F-62930 Wimereux, France*
[*]*Severine.alvain@univ-littoral.fr*

Abstract: Past years have seen the development of different approaches to detect phytoplankton groups from space. One of these methods, the PHYSAT one, is empirically based on reflectance anomalies. Despite observations in good agreement with *in situ* measurements, the underlying theoretical explanation of the method is still missing and needed by the ocean color community as it prevents improvements of the methods and characterization of uncertainties on the inversed products. In this study, radiative transfer simulations are used in addition to *in situ* measurements to understand the organization of the signals used in PHYSAT. Sensitivity analyses are performed to assess the impact of the variability of the following three parameters on the reflectance anomalies: specific phytoplankton absorption, colored dissolved organic matter absorption, and particles backscattering. While the later parameter explains the largest part of the anomalies variability, results show that each group is generally associated with a specific bio-optical environment which should be considered to improve methods of phytoplankton groups detection.

OCIS codes: (010.4450) Oceanic optics; (010.1690) Color; (010.1030) Absorption; (010.1350) Backscattering.

References and links

1. H. R. Gordon and A. Morel, *Remote Assessment of Ocean Color for Interpretation of Satellite Visible Imagery. A Review* (Springer-Verlag, New York, USA), 1983).
2. A. Morel, "Optical modeling of the upper ocean in relation to its biogenous matter content (case 1 water)," J. Geophys. Res. **93**(C9), 10,749–10,768 (1988).
3. S. Sathyendranath, L. Watts, E. Devred, T. Platt, C. Caverhill, and H. Maass, "Discrimination of diatoms from other phytoplankton using ocean-colour data," Mar. Ecol. Prog. Ser. **272**, 59–68 (2004).
4. A. Ciotti and A. Bricaud, "Retrievals of a size parameter for phytoplankton and spectral light absorption by Colored Detrital Matter from water-leaving radiances at SeaWiFS channels in a continental shelf region off Brazil," Limnol. Oceanogr. Methods **4**, 237–253 (2006).
5. J. Aiken, Y. Pradhan, R. Barlow, S. Lavender, A. Poulton, P. Holligan, and N. J. Hardman-Mountford, ""Phytoplankton pigments and functional types in the Atlantic Ocean: a decadal assessment, 1995-2005," Deep Sea Res. Part II Top. Stud. Oceanogr. **56**(15), 899–917 (2009).
6. S. Alvain, C. Moulin, Y. Dandonneau, and F. M. Breon, "Remote sensing of phytoplankton groups in case 1 waters from global SeaWiFS imagery," Deep Sea Res. Part I Oceanogr. Res. Pap. **52**(11), 1989–2004 (2005).
7. J. Uitz, H. Claustre, A. Morel, and S. B. Hooker, "Vertical distribution of phytoplankton communities in open ocean: An assessment based on surface chlorophyll," J. Geophys. Res. **111**(C8), C08005 (2006).
8. D. E. Raitsos, S. J. Lavender, C. D. Maravelias, J. Haralabous, A. J. Richardson, and P. C. Reid, "Identifying four phytoplankton functional types from space: An ecological approach," Limnol. Oceanogr. **53**(2), 605–613 (2008).
9. T. S. Kostadinov, D. A. Siegel, and S. Maritorena, "Retrieval of the particle size distribution from satellite ocean color observations," J. Geophys. Res. **114**(C9), C09015 (2009).
10. R. J. Brewin, S. Sathyendranath, T. Hirata, S. Lavender, R. M. Barciela, and N. J. Hardman-Mountford, "A three-component model of phytoplankton size class for the Atlantic Ocean," Ecol. Modell. **221**(11), 1472–1483 (2010).

#154226 - $15.00 USD Received 6 Sep 2011; revised 6 Nov 2011; accepted 10 Nov 2011; published 4 Jan 2012

11. J. E. O'Reilly, S. Maritorena, B. G. Mitchell, D. A. Siegel, K. L. Carder, S. A. Garver, M. Kahru, and C. McClain, "Ocean color chlorophyll algorithms for SeaWiFS," J. Geophys. Res. **103**(C11), 24,937–24,953 (1998).
12. Y. Dandonneau, P. Y. Deschamps, J.-M. Nicolas, H. Loisel, J. Blanchot, Y. Montel, F. Thieuleux, and G. Bécu, "Seasonal and interannual variability of ocean color and composition of phytoplankton communities in the North Atlantic, Equatorial Pacific and South Pacific," Deep Sea Res. Part II Top. Stud. Oceanogr. **51**(1-3), 303–318 (2004).
13. S. Alvain, C. Moulin, Y. Dandonneau, and H. Loisel, "Seasonal distribution and succession of dominant phytoplankton groups in the global ocean: A satellite view," Global Biogeochem. Cycles **22**(3), GB3001 (2008).
14. M. V. Zubkov, M. A. Sleigh, P. H. Burkill, and R. J. G. Leakey, "Picoplankton community structure on the Atlantic Meridional Transect: a comparison between seasons," Prog. Oceanogr. **45**(3-4), 369–386 (2000).
15. J.-C. Marty, J. Chiavérini, M.-D. Pizay, and B. Avril, "Seasonal and interannual dynamics of nutrients and phytoplankton pigments in the western Mediterranean Sea at the DYFAMED time-series station (1991–1999)," Deep Sea Res. Part II Top. Stud. Oceanogr. **49**(11), 1965–1985 (2002).
16. M. D. DuRand, R. J. Olson, and S. W. Chisholm, "Phytoplankton population dynamics at the Bermuda Atlantic time series station in the Sargasso Sea," Deep Sea Res. Part II Top. Stud. Oceanogr. **48**(8-9), 1983–2003 (2001).
17. A. Longhurst, *Ecological Geography of the Sea*, 2nd ed. (Academic, San Diego, Calif. (2007).
18. H. Loisel, B. Lubac, D. Dessailly, L. Duforet-Gaurier, and V. Vantrepotte, "Effect of inherent optical properties variability on the chlorophyll retrieval from ocean color remote sensing: an *in situ* approach," Opt. Express **18**(20), 20949–20959 (2010).
19. C. D. Mobley, *Light and Water: Radiative Transfer in Natural Waters* (Academic, San Diego, Calif., 1994).
20. C. Cox and W. Munk, "Measurement of the Roughness of the Sea Surface from Photographs of the Sun's Glitter," J. Opt. Soc. Am. **44**(11), 838–850 (1954).
21. C. D. Mobley, B. Gentili, H. R. Gordon, Z. Jin, G. W. Kattawar, A. Morel, P. Reinersman, K. Stamnes, and R. H. Stavn, "Comparison of numerical models for computing underwater light fields," Appl. Opt. **32**(36), 7484–7504 (1993).
22. A. Morel and S. Maritorena, "Bio-optical properties of oceanic waters: A reappraisal," J. Geophys. Res. **106**(C4), 7163–7180 (2001).
23. R. M. Pope and E. S. Fry, "Absorption spectrum (380-700 nm) of pure water. II. Integrating cavity measurements," Appl. Opt. **36**(33), 8710–8723 (1997).
24. R. C. Smith and K. S. Baker, "Optical properties of the clearest natural waters (200-800 nm)," Appl. Opt. **20**(2), 177–184 (1981).
25. A. Bricaud, A. Morel, M. Babin, K. Allali, and H. Claustre, "Variations of light absorption by suspended particles with chlorophyll a concentration in oceanic (case 1) waters: Analysis and implications for bio-optical models," J. Geophys. Res. **103**(C13), 31033–31044 (1998).
26. A. Bricaud, A. Morel, and L. Prieur, "Absorption by dissolved organic matter of the sea (yellow substance) in the UV and visible domains," Limnol. Oceanogr. **26**(1), 43–53 (1981).
27. A. Morel, "Are the empirical relationships describing the bio-optical properties of case 1 waters consistent and internally compatible?" J. Geophys. Res. **114**(C1), C01016 (2009).
28. D. A. Siegel, S. Maritorena, N. B. Nelson, and D. A. Hansell, "Global distribution and dynamics of colored dissolved and detrital organic materials," J. Geophys. Res. **107**(C12), 3228 (2002).
29. H. R. Gordon and A. Morel, *Remote Assessment of Ocean Color for Interpretation of Satellite Visible Imagery. A Review* (Springer-Verlag, New York, 1983).
30. H. Loisel and A. Morel, "Light scattering and chlorophyll concentration in case 1 waters: a re-examination," Limnol. Oceanogr. **43**(5), 847–858 (1998).
31. A. Morel, D. Antoine, and B. Gentili, "Bidirectional reflectance of oceanic waters: accounting for Raman emission and varying particle scattering phase function," Appl. Opt. **41**(30), 6289–6306 (2002).
32. H. Loisel, J.-M. Nicolas, A. Sciandra, D. Stramski, and A. Poteau, "Spectral dependency of optical backscattering by marine particles from satellite remote sensing of the global ocean," J. Geophys. Res. **111**(C9), C09024 (2006).
33. D. Antoine, D. A. Siegel, T. Kostadinov, S. Maritorena, N. B. Nelson, B. Gentili, V. Vellucci, and N. Guillocheau, "Variability in optical particle backscattering in contrasting bio-optical oceanic regimes," Limnol. Oceanogr. **56**(3), 955–973 (2011).
34. R. D. Vaillancourt, C. Brown, R. L. Guillard, and W. M. Balch, "Light backscattering properties of marine phytoplankton: relationships to cell size, chemical composition and taxonomy," J. Plankton Res. **26**(2), 191–212 (2004).
35. A. Bricaud, H. Claustre, J. Ras, and K. Oubelkheir, "Natural variability of phytoplankton absorption in oceanic waters: influence of the size structure of algal populations," J. Geophys. Res. **109**(C11), C11010 (2004).
36. H. Loisel and D. Stramski, "Estimation of the inherent optical properties of natural waters from irradiance attenuation coefficient and reflectance in the presence of Raman scattering," Appl. Opt. **39**(18), 3001–3011 (2000).
37. Y. Huot, A. Morel, M. Twardowski, D. Stramski, and R. A. Reynolds, "Particle optical backscattering along a chlorophyll gradient in the upper layer of the eastern south pacific ocean," Biogeosciences **5**(2), 495–507 (2008).
38. P. J. Werdell and S. W. Bailey, "An improved in-situ bio-optical data set for ocean color algorithm development and satellite data product validation," Remote Sens. Environ. **98**(1), 122–140 (2005).

#154226 - $15.00 USD Received 6 Sep 2011; revised 6 Nov 2011; accepted 10 Nov 2011; published 4 Jan 2012

1. Introduction

For a given chlorophyll a concentration (*Chl a*), phytoplankton groups scatter and absorb light differently according to their pigments composition, shape and size. However, the first order signal retrieved from ocean color sensors in open oceans, the normalized water leaving radiance (nLw), is due to *Chl a* [1,2]) and cannot be easily used to extract information about phytoplankton groups present in the oceanic surface layer. To circumvent this difficulty, different approaches have been developed in the past few years. When changes in nLw are significant enough between phytoplankton group, they can be detected from their specific radiances measurements [3,4]. When reflectance changes are not significant enough to separate one group from another one, empirical or semi-empirical methods have to be developed. This last case is particularly relevant when the objective is to detect groups defined from a biogeochemical or size point of view at global scale [5–10]. Note that 'phytoplankton groups' are defined here following the definition based on functional types, as detailed in a previously published article [6].

In this study, we will focus on the PHYSAT method (http://log.univ-littoral.fr/Physat) which allows the detection of dominant phytoplankton groups [6]. This approach is based on the analysis of the second order variation in nLw measurements after removal of the impact of chlorophyll *a* variation. Thus, PHYSAT is based on the reflectance anomalies, Ra(λ), computed as follows:

$$Ra(\lambda) = \frac{nLw(\lambda)}{nLw_{ref}(\lambda, Chl\ a)} \quad (1)$$

where nLw_{ref} (λ,*Chl a*) is calculated for discrete bins of chlorophyll *a* concentration and from remote sensed nLw measurements [6]. Briefly, nLw_{ref} is calculated from nLw data and the associated *Chl a* computed from the OC4v4 algorithm [11] within the following *Chl a* range: 0.02-3 $mg.m^{-3}$ with an increment of 0.1 $mg.m^{-3}$. This reference can then be used to remove the first order effect of chlorophyll *a* on nLw(λ) measurements. The second order variation is then represented by a new parameter, named Ra(λ) which, by definition, is independent of the *Chl a* level (being by extension independent of the biomass). Ra(λ) is an adimensional unit parameter.

Based on simultaneous *in situ* pigments inventories (mainly from the GeP&Co campaigns [12]) and remote sensing measurements collected by the SeaWiFS ocean color sensor, it has been shown that specific Ra(λ), in terms of magnitude and in a lesser extent of shape, are empirically associated with the following dominant groups: nanoeucaryotes, Prochlorococcus, Synecoccochus, diatoms and more recently Phaeocystis-like [13]. A set of criteria was defined in order to characterize each Ra(λ) spectra. These criteria can then be used to compute maps of dominant groups [6]. The geographical distribution and seasonal succession of each group have been studied using the global Sea-viewing Wide Field-of-view Sensor (SeaWiFS) archive [13]. These observations are in good agreement with previous studies based on *in situ* observations [12, 14–17]. Results of the last comparison between satellite and *in situ* biomarkers pigments observations are given in Table 1. Phaeocystis-like phytoplankton have not been considered in the present study due to scarce *in situ* information needed to support a robust validation at this stage. Results were satisfactory for diatoms (73% of good identification, based on biomarker pigments thresholds) and nanoeucaryotes (82% of successful identification), and a decrease in the percentage of successful retrieval was observed for Prochlorococcus and Cyanobacteria (respectively 61 and 57% of successful identification). This last result was expected since these two latter groups show similar characteristics (geographical distribution, size and specific Ra(λ) signal in PHYSAT).

While the spatial distribution of phytoplankton groups are generally consistent with our current knowledge, a theoretical frame explaining the empirical link between Ra(λ) and the

#154226 - $15.00 USD Received 6 Sep 2011; revised 6 Nov 2011; accepted 10 Nov 2011; published 4 Jan 2012

Table 1. Results of PHYSAT validation based on SeaWiFS daily measurements derived from the 2008 version of PHYSAT [13][a]

PHYSAT\ *IN SITU*	Nanoeucaryotes	Prochlorococcus	Cyanobacteria	Diatoms
Nanoeucaryotes	**82**	10	5	3
Prochlorococcus	14	**61**	25	-
Cyanobacteria	20	23	**57**	-
Diatoms	24	-	3	**73**

[a]For each group, the percentage of valid (bold) and wrong (others) identifications are shown. Wrong identifications are separated by groups.

dominant group is still missing and prevents futures improvements of the method. While the impacts of inherent optical properties (IOPs) on nLw have been widely studied in the past, this is not the case for the impact of specific phytoplankton groups' IOPs on Ra(λ). Indeed, the Ra(λ) organization according to phytoplankton groups (in terms of magnitude and slope) cannot be easily associated with specific size or IOP. Besides, the presence of other optically significant agents in the water, such as detritus and colored dissolved organic matter, may bias the detection of phytoplankton groups. Thus, a theoretical approach, based on numerical radiative transfer simulation and *in situ* measurements, is critical to improve the method and enable future developments. A better understanding of the impact of specific IOPs on Ra(λ) represents an opportunity to move forward in the domain of phytoplankton groups detection. Here we address this question using radiative transfer calculations in association with *in situ* pigments measurements.

2. Theoretical and computational considerations

The main objective of the numerical simulations is to test the sensitivity of the PHYSAT method, through the variability of Ra(λ), to the variability of inherent optical properties in case 1 water. We specifically focus on the effect of phytoplankton absorption, a_{phy}, particulate backscattering coefficient, b_{bp}, and absorption by colored dissolved organic matter, a_{cdom} (all these IOP are in m^{-1}). For that purpose, different sets of simulations have been performed.

2.1. Mean theoretical reference relationships

A first set of simulations (S1) (Fig. 1 step 2) is dedicated to the generation of a theoretical $nLw_{ref\text{-}theo}$ used to generate theoretical radiance anomalies (Ra_{theo}). This $nLw_{ref\text{-}theo}$ should match the nLw_{ref} obtained using the OC4V4 algorithm which is used in PHYSAT. Retrieval of *Chl* a from band ratio is affected by the natural variability of IOP's [18]. Mean IOP vs. *Chl* relationships have been fixed (Fig. 1 step 1) and numerical simulations have been performed to calculate a set of theoretical radiances corresponding to *Chl a* values ranging from 0.02 to 3 $mg.m^{-3}$ (range of the PHYSAT validity).

The radiative transfer equation is solved by the invariant embedding method using the Hydrolight 5.0 code [19]. All numerical simulations are carried out for a homogeneous and infinitely deep ocean. The air-sea interface is modeled following Cox and Munk [20] with a fixed wind speed of 5 $m.s^{-1}$. A standard clear atmosphere (with a visibility of 15 km) with a sun zenith angle at 30° is adopted. Raman scattering is taken into account in the simulations, whereas other inelastic processes (i.e. *Chl* a and CDOM fluorescence) are omitted. The molecular scattering phase function is calculated using theoretical consideration [21]. The particle phase function is derived from the formulation proposed by Mobley *et al*. [21], based on measurements by Morel and Maritorena [22]. Pure sea water absorption and scattering coefficients were taken from Pope and Fry [23] and Smith and Baker [24], respectively.

For a given wavelength the phytoplankton absorption coefficient, $a_{phy}(\lambda)$, is modeled as a function of *Chl* a as follows:

$$a_{phy}(\lambda) = A[Chl\,a]^{[E]} \quad (2)$$

#154226 - $15.00 USD Received 6 Sep 2011; revised 6 Nov 2011; accepted 10 Nov 2011; published 4 Jan 2012

A(λ) and E(λ) are the coefficients calculated by Bricaud et al., 98 [25] using a large data set of *in situ* measurements collected in oligotrophic, mesotrophic, and eutrophic oceanic waters. Absorption by colored dissolved organic matter is described according to [26, 27]:

$$a_{cdom}(\lambda) = 0.065[Chl\ a]^{0.75}\ \exp\left(-0.014(\lambda - 443)\right) \quad (3)$$

Note that absorption by detrital particles is not explicitly taken into account as it is characterized by a spectral shape similar to that of a_{cdom}, and it only represents on average 10% of a_{cdom} [28].

The particle scattering and its spectral dependency are expressed according to relationships based on previous works, Eq. (4) [22, 29–32]. The parameters have been slightly modified in order to minimize the difference between the simulated and PHYSAT reference spectra:

$$b_p(\lambda) = 0.30\ [Chl\ a]^{0.62}\left(\frac{\lambda}{660}\right)^{-\gamma} \quad (4)$$

where γ is the spectral slope which is modeled as a function of *Chl* a:

$$\gamma = -0.55 \log[Chl\ a] + 1.6 \quad (5)$$

This γ vs. *Chl a* relationship is very consistent with *in situ* measurements performed in the Mediterranean sea and in the Pacific ocean [33]. Note that because the particulate phase function is constant in the present study, variability of the particulate backscattering coefficient, b_{bp}, is directly related to that of b_{p}.

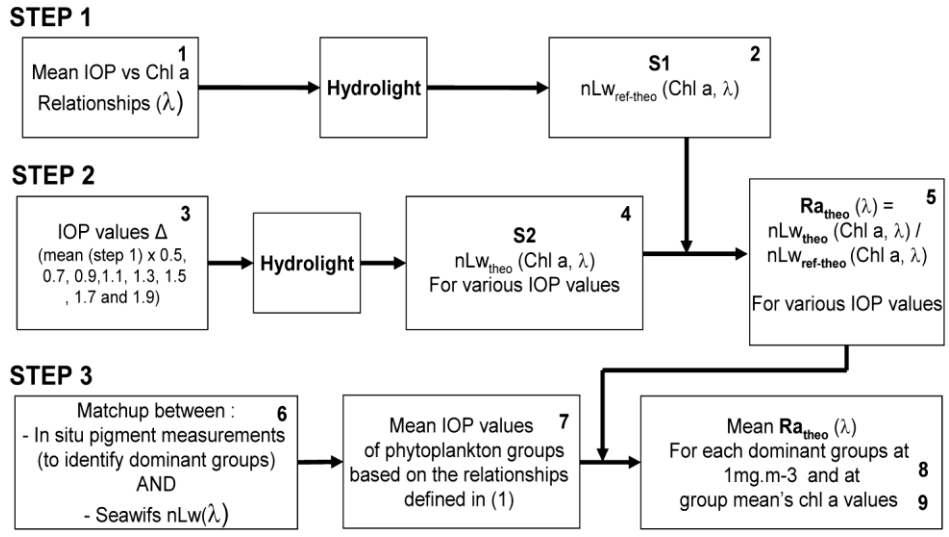

Fig. 1. Schematic view of steps followed to achieve theoretical analysis of ocean color radiances anomalies sensibility.

2.2. Set of nLw$_{theo}$ for various IOPs values

A second set of simulations (S2) is used to compute $\mathrm{nLw_{theo}}$ values for different IOP conditions (Fig. 1 step 4). In practice, two specific IOP are alternatively fixed while the third one is made variable as follows: for each IOP, its mean specific value (used to compute the S1 set) is multiplied by the following factors: 0.5 / 0.7 / 0.9 / 1.1 / 1.3 / 1.5 / 1.7 and 1.9. These factors allow to cover the specific IOP range of variability generally encountered in natural waters [34–36]. For each case, a simulation is made to generate the corresponding $\mathrm{nLw_{theo}}$

#154226 - $15.00 USD Received 6 Sep 2011; revised 6 Nov 2011; accepted 10 Nov 2011; published 4 Jan 2012

spectral values. These S2 simulations are performed for three different *Chl* a concentrations: 0.2, 1 and 2 $mg.m^{-3}$.

2.3. Phytoplankton groups and their associated bio-optical environment

A second focus of this study is to determine which set of IOP (and their given variability) better explains the organization in term of magnitude of the spectral radiance anomaly (i.e Ra(λ)) empirically determined for PHYSAT specific groups. To answer this question, it is necessary to define mean realistic ranges of IOP variability associated with the PHYSAT groups and their associated bio-optical environment. To remain as close as possible of PHYSAT conditions we will considered not only phytoplankton groups but phytoplankton groups in their realistic environment. Furthermore, considering the most recent validation of PHYSAT versus field observations (see introduction), this study will focus on the following three groups: diatoms, nanoeucayotes and a third one made by assembling Prochlorococcus and Cyanobacteria in a single group denominated Picoplanktonic cyanobacteria. This allows a theoretical analysis of the main groups associated with clearly different Ra *(λ) spectra in the empirically defined method.

Due to insufficient *in situ* measurements for the considered IOPs when considering each groups in dominance conditions, mean values associated with the three phytoplankton groups and their associated bio-optical environment have to be defined from the mean relationships established before (Eqs. (2)-(5)) and SeaWiFS sensors daily level 3 estimation of *Chl a* (9 km resolution) as input parameter (Fig. 1 step 6). *In situ* pigments inventories from NOMAD, GeP&CO, ICOTA 5 - 7 and OISO campaigns have been used for selecting only remote sensed measurements dominated by a specific group (Fig. 1 step 6). Note that the identification of the groups has been established by using the same biomarkers criteria than those established in the PHYSAT method [4]. Eventually, 527 inventories for which simultaneous high quality satellite matchup (aerosol optical thickness at 865 nm lower than 0.15 and *Chl a* values within the PHYSAT validity range) and *in situ* pigments inventories dominated by a single group have been considered.

Mean *Chl* a values were computed for each of the three phytoplankton groups considered from the match-up data points: 0.18 $mg.m^{-3}$ for Picoplanktonic cyanobacteria, 0.46 $mg.m^{-3}$ for nanoeucaryotes and 1.3 $mg.m^{-3}$ for diatoms. In order to avoid variations in $Ra_{theo}(\lambda)$ magnitude (for this test) related to changes *Chl* a loads, measurements within the interval corresponding to the group specific mean *Chl* a values ± 20% have only been selected. Considering such conditions, 22 observations for nanoeucaryotes, 14 for diatoms and 68 for Picoplanktonic cyanobacteria remain. For each of the selected pixels, mean bio-optical relationships (Eqs. (2)-(5)) have been used to derive IOPs values at each SeaWiFS wavelength. Mean IOPs values have then been computed for each group by averaging each group specific pixel subset (Fig. 1 step 7). These mean a_{phy}, a_{cdom} and b_p group-specific values have then been divided by the global mean IOPs values (obtained from all SeaWiFS *Chl a* estimation, with or without a dominant group, and Eqs. (2)-(5)) to define mean realistic IOPs ratios associated with each group and their specific bio-optical environment. These ratios, listed in Table 2, allow the assessment of the difference between overall and group specific IOP. Basically, waters dominated by Picoplanktonic cyanobacteria show the highest values of a_{phy}* (most likely due to the package effect), and the lower values for a_{cdom} and b_p (and b_{bp}) relatively to global mean values. Waters dominated by diatoms are associated with the highest b_p (and b_{bp}), as well as with the highest values for a_{cdom}. The b_{bp} values are coherent with laboratory studies performed on phytoplankton cultures, showing that the "mean" per-cell backscattering increases proportionally to the cell diameter [37]. For instance, diatoms are characterized by much higher backscattering cross-section than cyanobacteria. Conversely, waters dominated by diatoms are associated with the lowest values of a_{phy} * relatively to mean global values. Ratios in Table 2, calculated from previously defined relationships (Eqs. (2)-(5)), have been partially validated based on the NOMAD *in situ* database and some additional

#154226 - $15.00 USD Received 6 Sep 2011; revised 6 Nov 2011; accepted 10 Nov 2011; published 4 Jan 2012

cruises [38]. Indeed, after having considered all our criteria (*in situ* measurements with all IOPs, all biomarker pigments and case 1 water dominated by one group), 16 diatoms and 20 nanoeucaryotes assemblages were available. Unfortunately, no measurements associated with a Picoplanktonic dominance were found, thus preventing a direct validation of the values reported in the Table 2. However, the available information can be used as a first validation of ratio between diatoms and nanoeucaryotes parameters, as shown in Table 3. If the values from the two methods are not exactly the same, they are similar in terms of range of variation, diatoms being associated with higher values of a_{cdom} and b_p and lower values of a_{phy} *. This validation needs to be pursued as soon as additional *in situ* measurements for Picoplanktonic dominated waters will be available.

Table 2. Mean ratio of a_{phy}*, a_{cdom} and b_p for the mean *Chl a* values for each groups, relative to a reference computed from the mean relationships (used to parameterize Hydrolight) applied to all the *in situ* and SeaWiFS matchups available

	a_{cdom} group / a_{cdom} mean	a_{phy} * group / a_{phy}* mean	b_p group / b_p mean
Nano.	1.52	0.82	1.05
Pico. cyan.	0.8	1.3	0.85
Diat.	1.63	0.72	1.58

Table 3. Mean ratio of a_{phy}*, a_{cdom} and b_p values between diatoms and nanoeucaryotes phytoplankton groups, based on mean relationships (Eqs. (2)-(5)) and from *in situ* measurements

Based on \ Mean values of	$a_{cdom\ diatoms}$ / $a_{cdom\ nano.}$	$b_{p\ diatoms}$ / $b_{p\ nano.}$	$a_{phy*\ diatoms}$ / $a_{phy*\ nano.}$
Relationships	1.07	1.5	0.87
In situ measurements	1.16	1.3	0.91

3. Results and discussion

3. 1. Evaluation of the reference relationships

The first set of simulation (S1), based on averaged IOPs vs. *Chl* a relationships, is dedicated to the establishment of theoretical reference spectra close to those used in PHYSAT. Based on relationships detailed before, mean $nLw_{ref\text{-}theo}(\lambda)$ have been computed and can be compared to those used in the PHYSAT algorithm ($nLw_{ref\text{-}PHYSAT}(\lambda)$) (Fig. 2 and Table 4).

A good agreement is found between $nLw_{ref\text{-}theo}(\lambda)$ and $nLw_{ref\text{-}PHYSAT}(\lambda)$ in term of magnitude ranges. In addition, the consistency of the general parameterizations considered in this study (Eqs. (2)-(5)) is also tested through the development of a specific OC-MOD relationship. In practice, it is based on 4th order polynomial fit (to be consistent with OC4v4) between *Chl a* and the "maximum band ratio" of $nLw_{ref\text{-}theo}(\lambda)$:

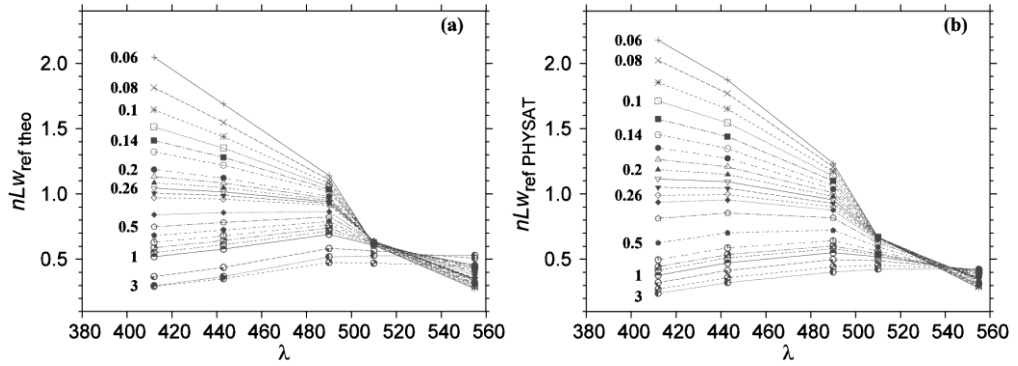

Fig. 2. (a) $nLw_{ref\text{-}theo}(\lambda)$ and (b) $nLw_{ref\text{-}PHYSAT}(\lambda)$ normalized radiance spectra for different Chl a values.

#154226 - $15.00 USD Received 6 Sep 2011; revised 6 Nov 2011; accepted 10 Nov 2011; published 4 Jan 2012

Table 4. Minimum and maximum values of the $nLw_{ref\text{-}theo}(\lambda)$ and $nLw_{ref\text{-}PHYSAT}(\lambda)$ normalized radiance spectra at each SeaWiFS wavelength

	412		443		490		510		555	
	Min	Max	Min	Max	Min	Max	Min	Max	Min	Max
$nLw_{ref\text{-}theo}$ (Hydrolight)	0.30	2.05	0.38	1.70	0.52	1.15	0.53	0.61	0.28	0.53
$nLw_{ref\ –PHYSAT}$ (PHYSAT)	0.36	2.3	0.50	1.90	0.65	1.32	0.68	0.75	0.3	0.72

$$\log(\text{Chl a}) = a\log^4(R) + b\log^3(R) + c\log^2(R) + d\log(R) + e \quad (6)$$

with

$$r = \frac{\text{Max}\left(R_{rs}(443), R_{rs}(490), R_{rs}(510)\right)}{R_{rs}(555)}$$

with R_{rs} the remote sensing reflectance ($R_{rs}(\lambda)=nLw(\lambda)/Fo(\lambda)$, with Fo the extraterrestrial irradiance).

This theoretical OC-MOD parameterization is compared with the OC4v4 empirical algorithm developed to assess *Chl* a concentration from the SeaWiFS ocean color sensor [11] and used as nLw_{ref} in Eq. (1) (Fig. 3). Over the PHYSAT *Chl* a range (0.02 - 3 $mg.m^{-3}$), the *Chl* a estimated from the OC-MOD algorithm is on average 17% greater than that derived from the OC4v4 formulation. In the context of this study and according to 1) the observed large scatter in the 'r vs *Chl* a' relationship in the NOMAD database [38] and 2) the overall agreement between the OC4v4 and OC-MOD mean relationships, such difference is considered as negligible (see Fig. 3).

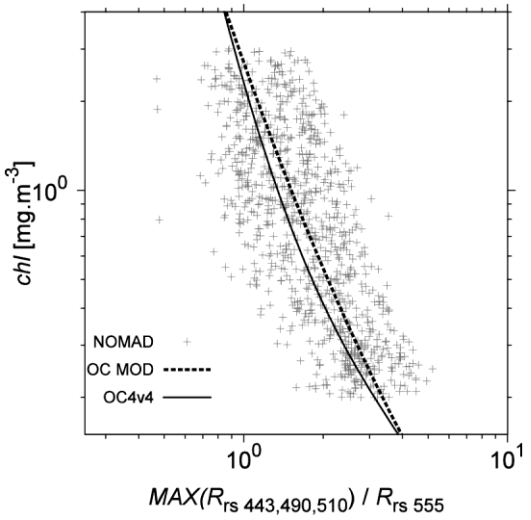

Fig. 3. Chl a as a function of the "maximum band" of the blue to green ratio r (see Eq. (6)) for the OC4v4 SeaWiFS algorithm (gray line, with a = –1.532,b = 0.649,c = 1.93,d = –3.067,e = 0.366 in Eq. (6)), Hydrolight output (black line, with a = 1.351,b = 0.301,c = –0.09,d = –2.37,e = 0.433 in Eq. (6)), superimposed with NOMAD [38] *in situ* measurements (light gray).

The S1 data set can be used to define a theoretical look up table (LUT) of $nLw_{ref\text{-}theo}$ for a given λ and *Chl a* (Fig. 1 step 2 and Fig. 2) similar to that used in PHYSAT. Further, the latter comparisons of absolute nLw_{ref} values (Fig. 2, and Table 4) and band ratios with a limited bias compared to *in situ* dispersion (Fig. 3) indicate that the different parameterizations adopted between the IOPs and *Chl* a (Eqs. (2)-(5)) are adapted to theoretically examine the

#154226 - $15.00 USD Received 6 Sep 2011; revised 6 Nov 2011; accepted 10 Nov 2011; published 4 Jan 2012

impact of different scenarios of IOP variability (the S2 simulations) on the radiance anomalies approach.

3.2. Evaluation of IOPs versus chlorophyll a relationships

In order to extend the previous theoretical results to realistic PHYSAT satellite observations, the mean semi-empirical relationships used to define our theoretical references (Eqs. (2)-(5)) are compared to the relationships established from the remote sensing inversed IOPs. For that purpose, we considered the data set of *in situ* pigments measurements and SeaWiFS daily matchup described previously. The particulate backscattering coefficient, $b_{bp}(\lambda)$, and the non-water absorption coefficient, $a_{nw}(\lambda)$, are retrieved from the improved version of the Loisel and Stramski (2000)'s model (Loisel et al; in preparation). Based on a synthetic data set (IOCCG, 2006) $b_{bp}(443)$ and $a_{nw}(443)$ are retrieved with a Root Mean Square error of 0.01 and 0.02, respectively. $a_{cdom}(\lambda)$ is simply assed by subtracting to $a_{nw}(\lambda)$ the particulate absorption coefficient, $a_p(\lambda)$, as estimated from Bricaud et al. (1998). The b_{bp} vs. *Chl a* and a_{cdom} vs. *Chl a* mean relationships (Eq. (3-4)) remarkably fall within the range of variability of the inversed (b_{bp}, *Chl a*) and (a_{cdom}, *Chl a*) data points (Fig. 4). Moreover, the behaviour of b_{bp} and a_{cdom} with *Chl a* changes as depicted by the regressions performed over the inversed data points, are relatively similar to the mean relationships. These results confirm the good agreement between the mean relationships used in this study and the match-up data set, and give us a certain confidence in the different IOPs ratio established for each group and their associated bio-optical environment (Table 2).

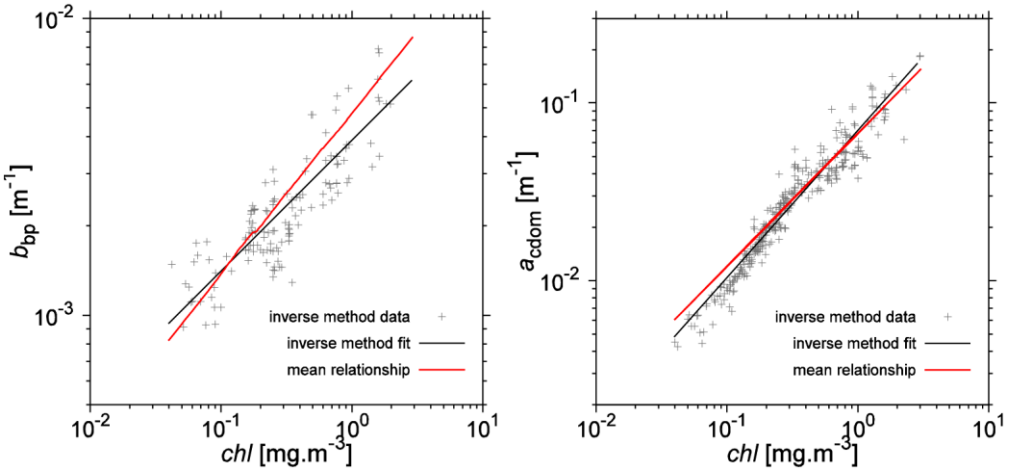

Fig. 4. Comparison of semi-empirically and from inversion defined relationships between a_{cdom} (a) or b_{bp} (b) and chlorophyll a concentration at 412 nm. Note that the bbp vs. Chl a mean relationship is established by multiplying the mean bp vs. Chl a relationship by 0.008 which represent the particulate backscattering ratio value used in the simulations.

3.3. PHYSAT signals response to IOPs variability

The aim of this section is to assess the impact of $a_{phy}^*(\lambda) = a_{phy}(\lambda)/Chl$ a, $a_{cdom}(\lambda)$ and $b_p(\lambda)$ (or b_{bp}) variability on $Ra_{theo}(\lambda)$.The $Ra_{theo}(\lambda)$ values are computed by dividing the $nLw_{theo}(\lambda)$ outputs from S2 by previously fixed $nLw_{ref\text{-}theo}(\lambda)$ in S1 (Fig. 1 step 5). Figures 5(a), (b) and (c) show, for three *Chl a* concentrations, the $Ra_{theo}(\lambda)$ spectra obtained when $a_{cdom}(\lambda)$, $a_{phy}^*(\lambda)$, and b_{bp} (λ) vary according to the different cases simulated in S2.

For a given chlorophyll concentration, variations in $a_{cdom}(\lambda)$ induce a large variability in $Ra_{theo}(\lambda)$, especially in the blue part of the spectrum (Fig. 5a). The $Ra_{theo}(\lambda)$ spectral shape depends strongly on the $a_{cdom}(\lambda)$ values. For low $a_{cdom}(\lambda)$ values, the $Ra_{theo}(\lambda)$ spectra decrease

#154226 - $15.00 USD Received 6 Sep 2011; revised 6 Nov 2011; accepted 10 Nov 2011; published 4 Jan 2012

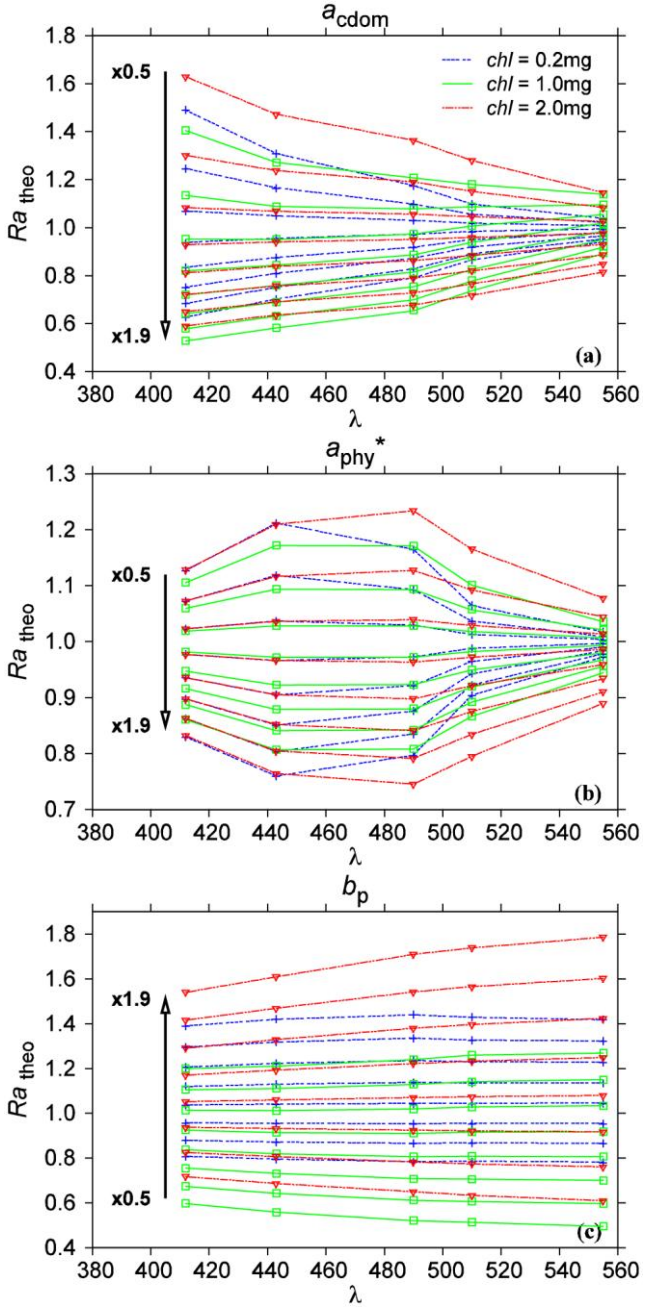

Fig. 5. Theoretical radiance anomalies as a function of wavelength in response to IOP (a_{phy}, a_{cdom} and b_p) variability, for three fixed chlorophyll concentration: 0.2 (blue lines), 1(green lines) and 2(red lines) mg.m^{-3}.

from the blue to red wavelengths, while they increase with λ for high $a_{cdom}(\lambda)$ values. The slope of the simulated $Ra_{theo}(\lambda)$ spectra is thus negative when a_{cdom} values are high, or positive when a_{cdom} values are low. At a given λ, the absolute value of $Ra_{theo}(\lambda)$ decreases when $a_{cdom}(\lambda)$ increases. This feature is valid for all *Chl a* values. However, $Ra_{theo}(\lambda)$ sensitivity to IOP variation is not exactly the same for all of the *Chl a*. At 412 nm, when the $a_{cdom}(412)$

#154226 - $15.00 USD Received 6 Sep 2011; revised 6 Nov 2011; accepted 10 Nov 2011; published 4 Jan 2012

value is twice or half of its mean value, the Ra_{theo} values range between 0.56 and 1.62, respectively.

Figure 5b shows the spectral response of $Ra_{theo}(\lambda)$ to the $a_{phy}^*(\lambda)$ variability. As expected, the highest $Ra_{theo}(\lambda)$ sensitivity is found at 443, where phytoplankton presents its main absorption peak. $Ra_{theo}(\lambda)$ values reach 1.22 when $a_{phy}^*(\lambda)$ is greater than its averaged value and decrease down to 0.76 when $a_{phy}^*(\lambda)$ is minimal ($a_{phy}^*(\lambda)$ mean value multiplied by 0.5). The lowest sensitivity is observed at 555 nm with a variation in the Ra_{theo} magnitude lower than 0.3 when $a_{phy}^*(\lambda)$ varies between its minimal and maximal value. As observed for the previous case-study (Fig. 4a), the sensitivity of $Ra_{theo}(\lambda)$ to $a_{phy}^*(\lambda)$ increases slightly with the *Chl a* concentration.

Unlike the two previous parameters, the $Ra_{theo}(\lambda)$ values increase with $b_p(\lambda)$ (Fig. 5c). Changes in $Ra_{theo}(\lambda)$ spectral shape associated with $b_p(\lambda)$ variation is restricted but the variation in the magnitude are greater than those observed for $a_{cdom}(\lambda)$ and $a_{phy}^*(\lambda)$. The $Ra_{theo}(\lambda)$ spectral values decrease to 0.56 when the $b_p(\lambda)$ value is half of its mean value, and increase to more than 1.8 when $b_p(\lambda)$ is maximal. Therefore, it appears that variation in $b_p(\lambda)$ (and thus in $b_{bp}(\lambda)$) is the main factor affecting the $Ra_{theo}(\lambda)$ absolute values. The latter feature is more nuanced in the blue part of the spectrum where $Ra_{theo}(\lambda)$ is equally affected by a_{cdom} and b_p. Similarly to $a_{phy}^*(\lambda)$ and $a_{cdom}(\lambda)$, the magnitude of $Ra_{theo}(\lambda)$ is sensitive to the chlorophyll *a* concentration. However, for a given chlorophyll *a* concentration, variations in IOPs lead to large $Ra_{theo}(\lambda)$ changes, independently of the *Chl a* variations.

3.4. Mean theoretical anomaly ($Ra_{theo}(\lambda)$) for each phytoplankton group

We have previously shown that, for a given Chl *a* concentration, variations in $a_{phy}^*(\lambda)$, $a_{cdom}(\lambda)$ and $b_p(\lambda)$ (i.e. $b_{bp}(\lambda)$) lead to various changes in $Ra_{theo}(\lambda)$. Interestingly, ranges of $Ra_{theo}(\lambda)$ variations obtained from the latter theoretical simulations (Fig. 5) are of the same magnitude than those observed from SeaWiFS measurements. Indeed, values of $Ra(\lambda)$ used in PHYSAT range between 0.6 to 1.8 at 412 nm, 0.75 to 1.5 at 443 nm and from 0.8 to 1.5 for longer wavelengths [13]. However, one may question whether these $Ra(\lambda)$ responses are sufficient to explain the distribution of the anomalies amplitudes observed in PHYSAT.

In order to test the impact of the different IOPs's groups ratios on $Ra_{theo}(\lambda)$, a first approach has been used with a single and realistic (based on our *in situ* data set) chlorophyll *a* concentration of 1 $mg.m^{-3}$ for all groups (Fig. 1 step 8). Ratios between mean specific $a_{cdom}(\lambda)$, $a_{phy}^*(\lambda)$ and $b_p(\lambda)$ values associated with each group have been previously computed (Table 2) and can be used to extract the corresponding $Ra_{theo}(\lambda)$ spectra in the S2 database (Fig. 5). The $a_{cdom}(\lambda)$ ratios values estimated for bio-optical environments dominated by diatoms or nanoeucaryotes lead to close and relatively low $Ra_{theo}(\lambda)$ spectra, with a positive spectral slope (Fig. 6a). Conversely, the relative low $a_{cdom}(\lambda)$ ratio value found in bio-optical environment dominated by Picoplanktonic cyanobacteria leads to higher $Ra_{theo}(\lambda)$ spectra with a negative slope. Variation in $a_{phy}^*(\lambda)$ leads to similar $Ra_{theo}(\lambda)$ spectral shape for both diatoms and nanoeucaryotes (Fig. 6b). However, a difference in $Ra_{theo}(\lambda)$ magnitude is observed with $Ra_{theo}(\lambda)$ for diatoms being higher than for nanoeucaryotes. The $a_{phy}^*(\lambda)$ ratio value found for bio-optical environment dominated by Picoplanktonic cyanobacteria leads to a rather flat $Ra_{theo}(\lambda)$ spectrum, with values lower than for the two previous groups (between 0.80 and 0.86). The $Ra_{theo}(\lambda)$ spectra associated with the $b_p(\lambda)$ ratio values are close for the nanoeucaryotes and Picoplanktonic cyanobacteria groups, and differ remarkably from those computed for diatoms (Fig. 6c). Indeed, the high specific $b_p(\lambda)$ values fixed for diatoms (Table 2) correspond to the highest $Ra_{theo}(\lambda)$ spectra (i.e. > 1.2 at every wavelength) while $Ra_{theo}(\lambda)$ values for the two others groups vary between 0.8 and 0.95.

In a second step, new radiative transfer simulations have been performed using both the mean group specific IOP and chlorophyll *a* concentration (Fig. 1 step 9). This has been done in order to assess the impact of the whole optical environment of each phytoplankton group

#154226 - $15.00 USD Received 6 Sep 2011; revised 6 Nov 2011; accepted 10 Nov 2011; published 4 Jan 2012

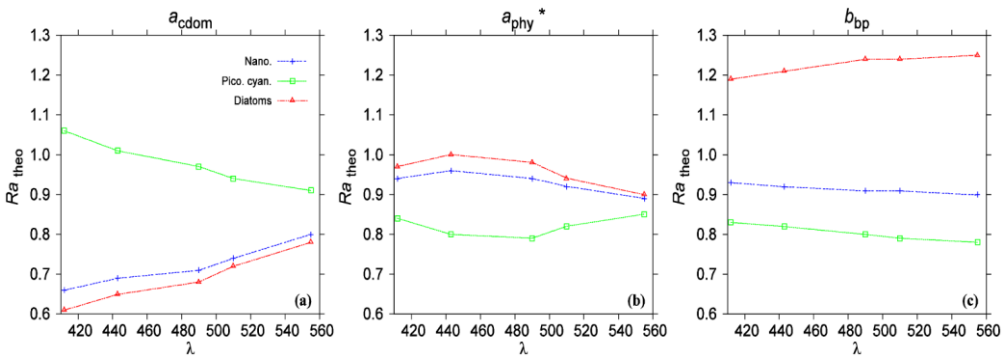

Fig. 6. Theoretical mean radiance anomalies as a function of wavelength, in response to variation in a_{cdom} (a), a^*_{phy}(b) and b_p(c) for a chlorophyll a concentration of 1mg.m^{-3}. Results are obtained for realistic parameters variations for the following phytoplankton groups: nanoeucaryotes (blue), picoplankton cyanobacteria (green) and diatoms (red).

(as defined in Table 2) on the $Ra_{theo}(\lambda)$ variability. The specific aim of this simulation was to tentatively explain the organization of the PHYSAT empirically defined spectra which cannot be explained considering each IOP separately.

Results of the simulation performed for each phytoplankton group show that the mean diatoms $Ra_{theo}(\lambda)$ spectrum presents greater values over the whole visible spectrum than those obtained for the two other bio-optical environments dominated by the two other groups (Fig. 7a). According to the previous sensitivity analysis (Fig. 6), this high $Ra_{theo}(\lambda)$ spectrum is mainly related to the high $b_p(\lambda)$ value associated with diatoms, which largely compensates the opposed effect of the relatively high $a_{cdom}(\lambda)$ value. Despite similar $a_{cdom}(\lambda)$ values associated with diatoms and nanoeucaryotes, the theoretical spectral radiance anomaly obtained for nanoeucaryotes is lower than that for diatoms. This is explained by the relatively low b_p value for nanoeucaryotes. At last, the $Ra_{theo}(\lambda)$ spectrum obtained for Picoplanktonic cyanobacteria represents an intermediate situation where the effect of the relatively low $a_{cdom}(\lambda)$ values (associated with the highest $Ra_{theo}(\lambda)$, see Fig. 6a) is compensated by the effect of $b_p(\lambda)$ and $a^*_{phy}(\lambda)$. Figure 7 shows that the $Ra_{theo}(\lambda)$ spectra of the different groups are organized in the same order, in term of magnitude, to that obtained empirically and defined in PHYSAT. Indeed, the lowest $Ra(\lambda)$ values are associated with a dominance of nanoeucaryotes, while the

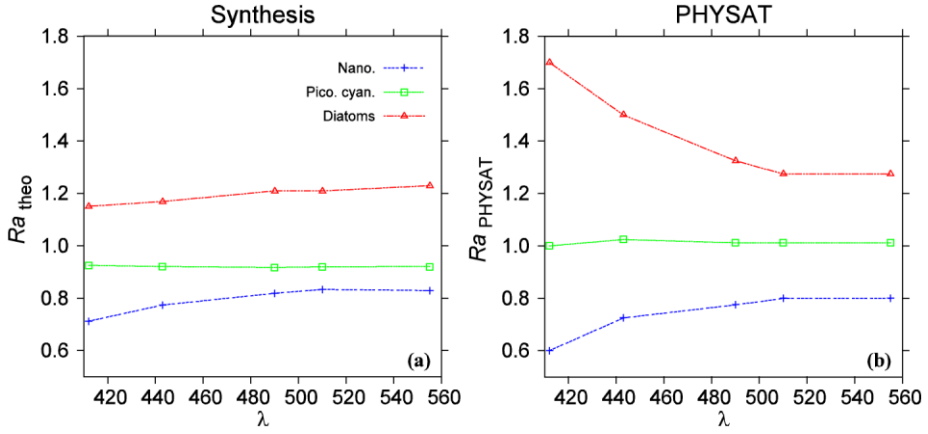

Fig. 7. Mean radiance anomalies for Nanoeucaryotes (blue), Picoplanktonic cyanobacteria (green) and diatoms (red) as a function of wavelength obtained theoretically (a) and observed empirically in PHYSAT (b).

#154226 - $15.00 USD Received 6 Sep 2011; revised 6 Nov 2011; accepted 10 Nov 2011; published 4 Jan 2012

highest values are obtained for diatoms [6]. This is the first time that a beginning of explanation of the Ra(λ) organization, entirely empirically defined before, is given.

The absolute values of the theoretical radiance anomalies for each groups slightly differ from the PHYSAT ones in terms of shape or amplitude. Thus, additional studies, based on large database of *in situ* IOP and radiometric measurements obtained during blooms corresponding to each phytoplankton group (not currently available for all groups), should be performed in the future to specifically address this issue.

3.5 Implications for PHYSAT in case 1 waters

Beyond the theoretical approach previously described and the first explanation of the distribution of Ra(λ), results obtained from the various simulations performed can also be used to evaluate the optimal conditions for PHYSAT application. Indeed, the bio-optical parameters associated with each of the three phytoplankton groups have been estimated from the mean bio-optical relationships described by Eqs. (2)-(5) and using *in situ Chl a* gathered in the database made of 527 inventories of simultaneous high quality satellite data and *in situ* HPLC measurements. Figure 8 shows that differences between the group-specific bio-optical environment illustrated by the relative contribution of a_{cdom}, b_p, and a_{phy}* are not systematic. These situations could lead to no-classification or misclassification of the radiometric signal in term of phytoplankton groups. For instance, the relative dominance between nanoeucaryotes and diatoms cannot be established when a relatively high contribution of a_{phy}* is found for these two groups. These specific conditions represent 34% and 9% of the measurements dominated by nanoeucaryotes and diatoms, respectively. However, most of these cases (93% for nanoeucaryotes and 75% for diatoms) lead to no-classification rather than to a misclassification. The remaining misclassification cases lead to wrong identification of Picoplanktonic cyanobacteria instead of nanoeucaryotes (7%) and identification of nanoeucaryotes instead of diatoms (25%). This result brings an essential explanation for wrong identifications found during the previous PHYSAT validation exercise [13]. In addition, some undetected dominance of diatoms can occur when the relative contribution of a_{cdom} to the three IOPs considered is higher than 26% and a_{phy}* contribution is very low (<4%) (Fig. 8). In this case, the b_{bp} contribution might be not sufficient enough to compensate the effect of a_{cdom} on the optical signal (Fig. 4).

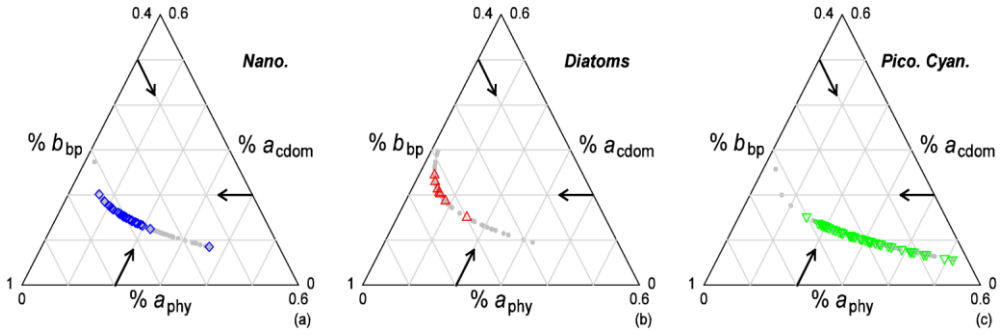

Fig. 8. Realistic view of a_{cdom} (horizontal lines), a_{phy}*(right tilt lines) and b_{bp} (left tilt lines) contribution at 412nm for waters dominated by nanoeucayotes (a), diatoms (b) or Picoplanktonic cyanobacteria (c). Gray points are those for which the considered group is dominant based on NOMAD pigments inventories and color points are those well identified by PHYSAT (nanoeucaryotes in blue, diatoms in red and Picoplanktonic cyanobacteria in green). The contribution of each IOP (%) is calculated by considering that the sum of each IOP (a_{cdom}, b_{bp} and a_{phy}) measurements assemblage is one and by computing the respective contribution of each parameter.

#154226 - $15.00 USD Received 6 Sep 2011; revised 6 Nov 2011; accepted 10 Nov 2011; published 4 Jan 2012

4. Conclusion and perspectives

The main purpose of this study was to theoretically analyze the bio-optical origin of the spectral shapes and amplitudes variability associated with each phytoplankton group detected by PHYSAT in case 1 waters. Indeed, after a necessary first step of development and validation of the PHYSAT method, a theoretical explanation of the empirical anomalies was strongly needed in order to move forward in the domain of phytoplankton groups detection. Thus, sensitivity analyses of the parameters used in PHYSAT Ra(λ), which varies almost independently of the biomass, were performed in function of IOPs. These analyses show that for a given chlorophyll concentration, the particle scattering variability explains the largest part of the remotely sensed Ra(λ) spectral variability, especially when focusing on Ra(λ) magnitude changes (Fig. 4). However, variations in colored dissolved organic matter and phytoplankton absorption coefficients can also have a large impact on Ra(λ) with specific spectral signatures. Following these sensitivity analyses, specific $Ra_{theo}(\lambda)$ spectra for bio-optical environment where the phytoplankton assemblage is dominated by diatoms, nanoeucaryotes and Picoplanktonic cyanobacteria have been computed. Diatoms are generally associated with high $Ra_{theo}(\lambda)$ due to high backscattering. Conversely, picoplankton is associated with mean $Ra_{theo}(\lambda)$ characterized by a high $a_{phy}(\lambda)$* compensated by low $a_{cdom}(\lambda)$ and $b_{bp}(\lambda)$ values. Nanoeucaryotes are associated with low $Ra_{theo}(\lambda)$ mainly due to high $a_{cdom}(\lambda)$ and moderate $b_{bp}(\lambda)$. The magnitude of the theoretically defined anomalies for the three groups is in good agreement with specific anomalies empirically highlighted and used in PHYSAT. Complementary studies, based on large *in situ* database of IOPs measurements, will be necessary in the future to improve our parameterizations in order to obtain a better agreement between the theoretical and PHYSAT spectral anomalies for the different groups. Unfortunately, such database is not yet available. However, this study provides some essential clues to explain the PHYSAT $Ra_{theo}(\lambda)$ differences between groups. This study represents a first step toward the theoretical understanding of PHYSAT results. It also opens new doors for improving phytoplankton groups detection. Thus, in a near future, the definition of the validity ranges for each group parameters (IOPs) will be integrated to the PHYSAT algorithm already published, in order to avoid misclassifications. Additional tests will also be processed from *in situ* and remotely sensed measurements in order to improve our knowledge on the optical conditions allowing the best detection for each group. This also opens new potential development by considering phytoplankton groups and their environmental conditions together.

Acknowledgments

The authors would like to thank all participants and voluntary contributors for collecting data that have been assembled in the NOMAD data set. They also thank organizers and observers of Gep&Co, OISO and ICOTA (and especially Dr A. Goffart) campaigns. The authors would like to thank the NASA SeaWiFS project and the NASA/GSFC/DAAC for the production and distribution of SeaWiFS data. We also thank Dr A. Bricaud for providing her parameters. We are also grateful to our funding sources, the CNRS, the CNES-TOSCA/PHYTOCOT project and the INTERREG IV—2 MERS SEAS ZEEN program. Dr. E. Boss and two reviewers are acknowledged for their relevant comments and suggestions on the manuscript.

#154226 - $15.00 USD Received 6 Sep 2011; revised 6 Nov 2011; accepted 10 Nov 2011; published 4 Jan 2012